Earth Syst. Sci. Data, 10, 627–641, 2018
https://doi.org/10.5194/essd-10-627-2018

Open Access Earth System Science Data

Hydrography and biogeochemistry dedicated to the Mediterranean BGC-Argo network during a cruise with RV *Tethys 2* in May 2015

Vincent Taillandier[1], Thibaut Wagener[2], Fabrizio D'Ortenzio[1], Nicolas Mayot[1,a], Hervé Legoff[3], Joséphine Ras[1], Laurent Coppola[1], Orens Pasqueron de Fommervault[1,b], Catherine Schmechtig[4], Emilie Diamond[1], Henry Bittig[1], Dominique Lefevre[2], Edouard Leymarie[1], Antoine Poteau[1], and Louis Prieur[1]

[1]Sorbonne Universités, UPMC Université Paris 06, CNRS, LOV, Villefranche-sur-Mer, 06230, France
[2]Aix-Marseille Universiteì, CNRS/INSU, Universiteì de Toulon, IRD,
Mediterranean Institute of Oceanography (MIO), UM 110, Marseille, 13288, France
[3]Sorbonne Universités, UPMC Univ Paris 06, CNRS, IRD, MNHN, LOCEAN, Paris, France
[4]Sorbonne Universités, UPMC Univ Paris 06, CNRS, UMS 3455, OSU Ecce-Terra, Paris CEDEX 5, France
[a]now at: Bigelow Laboratory for Ocean Sciences, Maine, East Boothbay, USA
[b]now at: Laboratorio de Oceanografià Fisicà, CICESE, Ensenada, B.C., Mexico

Correspondence: Vincent Taillandier (taillandier@obs-vlfr.fr)

Received: 23 October 2017 – Discussion started: 6 November 2017
Revised: 14 February 2018 – Accepted: 23 February 2018 – Published: 28 March 2018

Abstract. We report on data from an oceanographic cruise, covering western, central and eastern parts of the Mediterranean Sea, on the French research vessel *Tethys 2* in May 2015. This cruise was fully dedicated to the maintenance and the metrological verification of a biogeochemical observing system based on a fleet of BGC-Argo floats. During the cruise, a comprehensive data set of parameters sensed by the autonomous network was collected. The measurements include ocean currents, seawater salinity and temperature, and concentrations of inorganic nutrients, dissolved oxygen and chlorophyll pigments. The analytical protocols and data processing methods are detailed, together with a first assessment of the calibration state for all the sensors deployed during the cruise. Data collected at stations are available at https://doi.org/10.17882/51678 and data collected along the ship track are available at https://doi.org/10.17882/51691.

1 Introduction

1.1 Context of the cruise

The biogeochemical functioning of the Mediterranean Sea is typical of temperate oceanic regions. Seasonal dynamics of phytoplankton follow an increase of biomass in spring even if primary production remains low during the whole year (Marty et al., 2002). The biomass distribution in the Mediterranean Sea is marked by a pronounced east–west gradient (Bosc et al., 2004). This pattern is confirmed by the phenology of the underlying phytoplankton dynamics that varies from ultra-oligotrophic regimes in the eastern basin to bloom regimes in the northwestern basin (D'Ortenzio et al., 2009). An extended study on the geographical distribution of these regimes – related to the Mediterranean bio-regions – has revealed significant changes at regional scales during the last decades (Mayot et al., 2016). Indeed, the seasonal cycle of biomass concentration turns out to be a reliable indicator of the response of pelagic ecosystems to external perturbations (Siokou-Frangou et al., 2010). Facing increasing anthropogenic effects and considered to be a regional hotspot where climate change impacts will be the largest (Giorgi and Lionello, 2008), it would appear to be essential to characterize this indicator in the Mediterranean Sea basin under a

large panel of possible trophic regimes and various physical and chemical environments (Durrieu de Madron et al., 2011).

The seasonal cycles of biomass concentration have mainly been observed from satellite images of ocean color, thanks to their synoptic coverage of the area. Although limited to surface characterization, the link between biomass structuration in the water column and the underlying physical–chemical state over a seasonal scale has only been found at few ocean observation sites (Marty and Chiaverini, 2010). The emergence of BGC-Argo floats, which are autonomous profiling platforms equipped with biogeochemical sensors and programmed at weekly cycles up to 1000 m depth (Leymarie et al., 2013), now allows us to collect oceanographic profiles concomitantly for physical and biogeochemical properties (temperature, salinity, concentration of dissolved oxygen, chlorophyll *a*, nitrate). These open new perspectives for the description and comprehension of the biogeochemical functioning of the Mediterranean Sea. For example, the occurrence of phytoplankton blooms can be directly related to the availability of nutrients (D'Ortenzio et al., 2014).

Such technological advances have driven the development of a dedicated observing system over the Mediterranean Sea with a fleet of a dozen BGC-Argo floats in operation. This emerging network has been promoted and sustained by French programs such as Equipex-NAOS and the Mermex experiment, as well as at the European level through Euro-Argo infrastructure. However, sensors for biogeochemical properties, even with recent factory calibration, are subject to substantial systematic errors when deployed on BGC-Argo floats, as reported by Bittig et al. (2012) for oxygen measurements or by Pasqueron de Fommervault et al. (2015) for nitrate measurements. As a consequence, even if a BGC-Argo float is supposed to be completely autonomous after deployment, reference data for quality assessment of most of its sensors need to be collected by ship (D'Ortenzio et al., 2014; Johnson et al., 2017). Automatic quality controls are rapidly advancing for the Argo program (Schmechtig et al., 2015), although most of the methods and protocols are still under assessment. In this context, dedicated and precise efforts were necessary to ensure data quality of the Mediterranean observing system composed of BGC-Argo floats.

1.2 Objectives and achievements of the cruise

The data set presented in this paper was collected during an oceanographic cruise carried out in spring 2015 over the Mediterranean Sea. To our knowledge, it was the first cruise fully dedicated to the maintenance and the metrological verification of an autonomous observing system based on BGC-Argo floats. The objectives of the cruise were twofold: (1) to continue the time series of profile collection in operation since 2012 in the Mediterranean Sea, by deploying new BGC-Argo floats and recovering old ones and (2) to harmonize this collection with the systematic verification of calibration states for all biogeochemical sensors active in the network, using shipboard measurements as reference standards.

The choice of a dedicated cruise instead of ships of opportunity was driven by applying the same protocol of metrological verification for all the floats, using the same instruments and methods of reference. Another crucial point remains the required flexibility to choose the location of the oceanographic stations, which mainly depended on the state of the network (i.e., the position of the different floats) at the time of the cruise.

The survey covered large parts of the western, central and eastern basins of the Mediterranean Sea with a total route of about 3000 nm (Fig. 1). The cruise started in Nice (France) on 12 May 2015 and ended up in Nice on 1 June 2015, on board the *Tethys 2*, a 24 m long research vessel of the French National Center for Scientific Research (CNRS), comprised of a crew of seven and five scientists. The cruise was divided into four legs of about 4 days each with three port calls were programmed: 18–19 May in Heraklion (Crete, Greece), 24–25 May in Heraklion and 28–29 May in Lipari (Sicily, Italy). The initial cruise planning settled upon seven oceanographic stations, which represents about two stations for each 10 h leg. Transects between stations were crossed at 8–11 kn depending on sea conditions.

Work on board during the transects was dedicated to the surface sampling, together with seawater sample analyses and data processing. During stations, a CTD carousel composed of 11 Niskin bottles was deployed and discrete samples were collected for one shallow cast (0–500 dbar) and one deep cast (0–bottom). Standard levels were chosen for the deep cast (bottom, 2000, 1500, 1250, 1000, 750, 500 dbar; salinity maximum, 200 dbar; chlorophyll maximum, 10 dbar). The shallow cast was composed of six standard levels (500, 200, 150, 50, 10, 5 dbar) and five levels dedicated to the sampling of the deep chlorophyll maximum. This sampling strategy was reduced to a single cast (0–1000 dbar) in case of rough sea conditions, or extended with another cast (0–1000 dbar) for calibration purposes. The number of casts and samples are summarized in Table 1, with a total of 60 pigment samples, 148 oxygen samples and 154 nutrient samples.

The cruise was prepared in coordination with the Euro-Argo infrastructure so that series of Argo and BGC-Argo floats were provided by different European institutes (BSH Germany, OGS Italy, LOV France). Herein, only the BGC-Argo component is considered. At the time of the cruise, there were 12 active floats; 4 of these floats were recovered and 10 new floats were deployed during the cruise. The standard method consisted of deploying BGC-Argo floats at the end of every station, as listed in Table 2. Calibration exercises were created assuming that the CTD casts and the first float profiles could be considered co-located in time and space. That is why the floats were programmed to profile everyday at noon at the beginning of their mission. The first deep profile (0–1000 m) acquired by the floats occurred on the day of

Table 1. Station summary. For bottom depth, values with asterisk indicate that the measurement was obtained from the vessel's echo-sounder rather than the altimeter interfaced to the CTD unit.

Station	Cast	Date/time UTC DD/MM/YY	Latitude	Longitude	Profile depth (m)	Bottom depth (m)	No. of samples, pigments	No. of samples, oxygen	No. of samples, nutrients
Ligurian	1	12/05/15 20:10	43°33.52′ N	7°27.78′ E	1662	1684	5	11	11
North Ionian	2	16/05/15 03:41	38°10.44′ N	18°30.12′ E	500	3038	8	5	11
	3	16/05/15 05:35	38°10.96′ N	18°30.16′ E	2990	3038	0	11	11
Central Levantine	4	21/05/15 12:21	33°33.90′ N	28°27.99′ E	500	2959*	8	11	11
	5	21/05/15 14:14	33°33.76′ N	28°28.50′ E	1240	2959*	0	11	11
West Levantine	6	22/05/15 10:33	34°13.89′ N	24°49.84′ E	1000	2244*	7	11	11
	7	22/05/15 15:02	34°12.61′ N	24°50.76′ E	500	2886	8	11	11
	8	22/05/15 17:04	34°12.66′ N	24°50.56′ E	2871	2886	0	11	11
East Ionian	9	26/05/15 12:51	36°41.84′ N	20°07.32′ E	500	3175	8	11	11
	10	26/05/15 14:44	36°41.57′ N	20°07.21′ E	3165	3175	0	11	11
South Tyrrhenian	11	30/05/15 10:05	39°10.43′ N	10°53.47′ E	500	2812	8	11	11
	12	30/05/15 13:36	39°11.44′ N	10°52.37′ E	2803	2812	0	11	11
Central Tyrrhenian	13	31/05/15 05:21	40°45.22′ N	11°30.28′ E	500	2466	8	11	11
	14	31/05/15 07:14	40°45.87′ N	11°30.66′ E	2456	2466	0	11	11

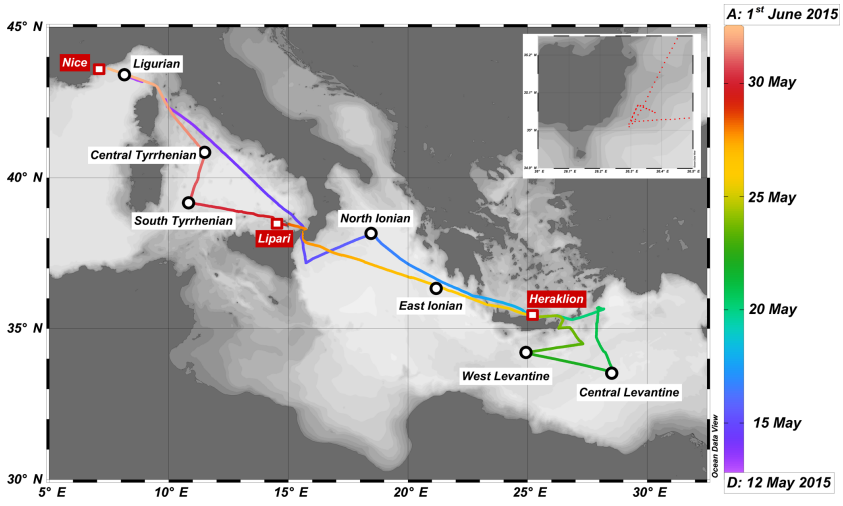

Figure 1. Cruise track plotted on a time line (color bar). Port calls are marked by red squares, and stations are marked by black circles. Detail of the L-shape track in the eastern coast of Crete.

the station if deployed early in the morning, or the day after if deployed later, as reported in Table 2.

This protocol of deployment is effective if working clearance in the area of the station was obtained in order to perform CTD casts. Unfortunately, this was not the case in the eastern Levantine Basin where the definitions of maritime exclusive economic zones are still vague. As a consequence, one BGC-Argo float was deployed without any reference CTD cast in the eastern Levantine (out of the list reported in Table 2). Two other floats were deployed in the same area some days after in the same conditions; however, the calibration exercise was performed at the west Levantine station by clamping the floats onto the frame of the CTD carousel and acquiring a profile (identified as BCN in Table 2) concomitant with the reference CTD profile and discrete samples.

The aims of this paper are to describe the collected data set. The sensing means and the underlying processing tools for data acquired from the ship and from BGC-Argo floats are detailed in the next section. The description and the instructions on accessing the quality-controlled data set are provided. Finally, a discussion follows about the various methodological strategies to update the BGC-Argo network in the Mediterranean Sea and to provide in situ calibration of the sensors.

Table 2. BGC-Argo float summary. For every BGC-Argo float deployed with a CTD cast of reference, the distance and duration with the first profile of the float are indicated. The results of metrological verification by parameter are reported. SD stands for standard deviation. PSAL: practical salinity.

Station	ARGO WMO	First profile ID	Inter-distance (km)	Inter-duration (h)	Temp offset (°C)	PSAL offset	Optode slope	Optode offset ($\mu mol\,kg^{-1}$)	Fluo N	Fluo R^2	Fluo offset ($mg\,m^{-3}$)	Fluo slope	SUNA slope	SUNA offset ($\mu mol\,L^{-1}$)
West Lev.*	6901764	BCN	0	0	0.0059	0.0150	0.9796	11.56	7	0.98	0.01	0.67	1.00	3.20
West Lev.	6901765	000	1	19	0.0003	0.0031	1.0660	3.26	8	0.77	0.04	0.62	1.00	4.00
West Lev.*	6901766	BCN	0	0	0.0053	0.0081	1.0275	6.30	7	0.98	−0.02	0.65	1.11	0.80
Central Tyr.	6901767	000	3	7					8	0.86	0.03	0.49	1.00	−2.80
Central Tyr.	6901767	001	3	29	0.0021	−0.0009	1.1045	−3.59					1.00	−2.70
North Ion.	6901768	001	12	31	0.0052	0.0009	1.0235	6.66	8	0.89	0.04	0.63	1.00	2.10
South Tyr.	6901769	000	2	26	0.0214	0.0050	1.1626	−14.87	8	0.82	0.03	0.58	1.00	3.90
East Ion.	6901771	000	2	21	0.0085	0.0042	1.0658	0.51	8	0.93	0.02	0.55	1.17	0.10
Central Lev.	6901773	000	3	22	0.0067	0.0070	1.0923	−2.40	8	0.99	0.01	0.51		
Average			3	17	0.0069	0.0053	1.0652	0.93			0.02	0.59	1.04	1.08
SD			4	12	0.0064	0.0049	0.0564	8.12			0.02	0.07	0.07	2.74

* Metrological verification exercise: deployed at another location than the station.

2 Methods for sensing, processing and quality control

The method employed for measurement (sensor technology, analytical protocol), the method used to process the collected data, and the operated quality control on the final data set is then presented per parameter (or family of parameters).

2.1 Ocean currents

2.1.1 Presentation of the different measurements

Ocean currents were measured with acoustic Doppler current profilers (ADCP), along the ship track and at every station using two dedicated instruments.

The vessel has been equipped since January 2015 with an Ocean Surveyor 75 kHz interfaced with a GPS and a gyro-compass. For the cruise, the ship ADCP (hereafter SADCP) was programmed in broadband single-ping profile mode, over 70 bins of 8 m and a blanking distance of 8 m. The maximum range obtained was 500 m; it was reduced to 250 m in the ultra-oligotrophic waters of the eastern basin.

The CTD carousel was equipped with a lowered ADCP (hereafter LADCP) system. It was composed of two RDI Workhorse Monitors 300 kHz, one uplooker was clamped onto the upper part of the frame that removed one over 12 Niskin bottles, and one downlooker clamped onto the lower frame. The two sensors were synchronized by a command WM15. The system was supplied by an external battery box installed in the lower frame. The LADCP was programmed in narrowband mode with a sampling rate of 1 Hz and 20 bins of 8 m and a blanking distance of null, Earth coordinate which tilts the three-beam solution, and bin mapping.

2.1.2 Data processing

Data flow from SADCP was archived on board and pre-processed using the manufacturer's software VMDAS, providing 2 min averaged velocity profiles. At least once per day, the data collection was uploaded and processed using the software Cascade V6.2 (Le Bot et al., 2011): ocean currents were generated by correcting raw velocity profiles from the ship navigation and attitude. Bottom detections were masked using GEBCO 1' bathymetry, corrections of ocean tides were not applied. Two data sets were assembled: one set with a time resolution of 2 min for ocean current profiles acquired during stations, one set with a spatial resolution of 1 km for ocean current profiles acquired during transits.

Data flow from LADCP system was processed using the software LDEO IX (Thurnherr, 2014). The architecture of this software allows us to replay the processing chain with different parameterizations: depth computation either from bottom track or by using the concomitant CTD profile, the threshold of percentage of good values, the assimilation of SADCP data and the weight of this constraint, either time resolution (1 s nominal) or vertical resolution (5 m bins), adjustment of the variation of magnetic declination.

LADCP data were processed with different levels of complexity. Right after each cast, a first screening of measurements was performed in order to validate the functioning of the system and assess the percentage of good values. When CTD profiles were available, a first ocean current profile was computed with refined depth constraint. In a final step, the misfit with a mean SADCP profile during station was attempted to be minimized by iteratively processing LADCP data with this new constraint.

2.1.3 Data quality control

An in situ calibration of SADCP sensor was undertaken during the cruise. An L shape of 10 nmi length was crossed back

and forth by the ship in calm seas and at moderate speeds over a shallow area off the eastern coast of Crete (see Fig. 1). Bottom track was acquired all the time which allowed comparison of ocean currents during the way in and the way back, supposedly steady over the 2 h duration of the exercise. The two transects were significantly different in amplitude and azimuth. Corrections on misalignment angle (1.1°), amplitude factor (1.004) and pitch thresholds (1 and 1.5°) for the SADCP were proposed in order to reduce the misfits between transects. Note that this calibration exercise would not have been necessary using CODAS software, which allows computation of the SADCP misalignment angle. Quality-controlled data sets of ocean currents along the ship track were post-processed thanks to these corrections.

This post-processed SADCP data set was also examined during stations in order to assess and improve the quality of the 14 LADCP profiles. As reported in Table 3, all the profiles except at casts 3 and 10 are characterized by low velocity errors and acceptable misfits with SADCP profiles. The median value of these uncertainties over the 12 acceptable casts using 1 s resolution profiles (approximately 800 ensembles) was evaluated to $-0.94 \pm 3.1\,\mathrm{cm\,s^{-1}}$ in module and $5.4 \pm 38°$ in azimuth without the SADCP constraint. Under SADCP constraint the median value reaches $0.17 \pm 1.1\,\mathrm{cm\,s^{-1}}$ in module and $-0.02 \pm 23°$ in azimuth. It is shown that the SADCP constraint does not significantly improve the ocean current estimate in module, but does at azimuth. The quality-controlled data set of ocean currents collected at the stations was processed with SADCP constraint and binned at 5 m resolution.

2.2 Seawater temperature and practical salinity

2.2.1 Presentation of the different measurements

Temperature and practical salinity properties of seawater were continuously measured at surface along the ship track by the underway system of the vessel, and at depth by the underwater unit or by the BGC-Argo floats during the seven stations.

A SeaCAT thermosalinograph (SBE21, serial no. 3146), hereafter TSG, was mounted in the underway system of the vessel. This instrument is composed of a conductivity cell and a local temperature probe in order to derive practical salinity. A remote temperature probe (SBE38, serial no. 0528) interfaced with the TSG was located at the inlet of the underway flow to minimize thermal contamination. Factory calibration of the TSG system was performed within the year preceding the cruise (29 July 2014). The acquisition started on 13 May 00:00 UTC, and it was halted during port calls.

The underwater unit was equipped with a CTD (SBE911+, serial no. 0329), which contained an internal pressure sensor, an external temperature probe (SBE3plus, serial no. 2473) and an external conductivity cell (SBE4C, serial no. 1313). A factory calibration of the two sensors was performed within the month preceding the cruise (16 April 2015). The GO-SHIP guidelines (Hood et al., 2010) were followed for the preparation, maintenance and deployment procedure of this instrument package.

The BGC-Argo floats were equipped with factory-calibrated CTD modules (SBE41CPs). These modules are designed as for mooring sensors to guarantee long-term stability of temperature, conductivity and pressure measurements. The probes were plumbed in a U-shaped seawater circuit with pump entrainment and taped with anti-foulant devices.

2.2.2 Data processing

The TSG data flow of 15 s resolution was archived on board together with GPS data flow as unmodifiable hexadecimal encoded files. At least once per day, the data collection was processed to feed a single time series of 5 min resolution for UTC time, geolocation, temperature and practical salinity.

During stations, seawater properties were sampled at 24 Hz with the CTD unit and transmitted on board through an electro-mechanical sea cable and slip-ring-equipped winch. At-sea processing of the archive was run after each CTD cast following GO-SHIP guidelines (Hood et al., 2010).

Data from BGC-Argo floats were transmitted to land via satellite Iridium communication and disseminated by a dedicated server. Continuous acquisition at 0.5 Hz was performed during the ascent phase of the float; pressure, temperature and practical salinity were then processed before transmission following user specifications: in the pressure range 0–10 dbar, the nominal resolution is kept; in the pressure range 10–250 dbar, averages of 2 dbar slices were computed; in the pressure range of 250–1000 dbar, averages of 10 dbar slices were computed.

2.2.3 Data quality control

The pressure measured from the CTD unit was compared on the vessel's deck with a barometer reading during port calls. No significant shift was observed that would require a post-cruise adjustment of this sensor.

There were no independent samples (such as salinity bottles) or double probes in the CTD unit that would have allowed the assessment of the temperature and conductivity sensors' stability. Thus, the quality of CTD data relies on frequent factory calibrations operated on the sensors: a pre-cruise bath was performed in April 2015 (less than 1 month before the cruise), and a post-cruise bath performed in March 2016 (less than 1 year after the cruise). The static drift of the temperature sensor between baths was 0.00008 °C which is 1 order of magnitude lower than the theoretical stability of the probe. The static conductivity ratio between baths was 1.0000321 which represents a drift of about $0.0015\,\mathrm{mS\,cm^{-1}}$, 1 order of magnitude lower than the theoretical stability of the probe. Given the reproducibility

Table 3. Summary of ocean current profiles collected at the stations. Depth and bottom track (BT) distances, when available, are indicated. Error velocities were computed for three sets of profiles: LADCP (L) data only, SADCP (S) data only and L data processed under the constraint of S data. Final process parameters were chosen as a function that leads to the misfits between L (with final process parameters) and S currents.

Cast	Depth (m)	BT distance (m)	Error velocity ($cm\,s^{-1}$) L without S constraint	Error velocity ($cm\,s^{-1}$) L with S constraint	Error velocity ($cm\,s^{-1}$) S	LDEO final parameters	Misfits L ms S ($cm\,s^{-1}$)	Comments
1	1721	26	2.5	2.5	5.5	L + S + BT	1.8	
2	498		3.4	3.4	5.7	L + S	3.8	
3	2990	53	20.3	18.9	6.5	L + S + BT	19.2	rough sea, high tilt
4	501		3.1	2.3	6.9	L + S	3.1	
5	1243		2.9	3.4	6.4	L + S	6.9	
6	996		2.5	2.6	5	L + S	2.0	
7	496		2.5	2.4	4.6	L + S	2.2	
8	2871	16	2.9	4.8	4.7	L + S + BT	6.1	
9	502		2.2	3.1	4.5	downlooker + S	2.6	uplooker failed, low battery
10	3165	17	20.7	50.4	5.2	downlooker + S + BT	36.0	
11	497		3	3	5.9	L + S	4.5	
12	2805	7	5.4	4.2	6.1	L + S + BT	4.4	
13	505		2.6	2.5	5	L + S	2.5	
14	2456	12	2.8	2.8	5.3	L + S+ BT	3.6	

of the processing method, the uncertainties of measurement provided by the CTD unit should have stayed within the accuracy of the sensors, which is 0.001 °C and 0.003 mS cm^{-1} out of lowered dynamic accuracy cases (such as in sharp temperature gradients).

The data collection of temperature and practical salinity profiles at every station is thus used as reference to assess the two other sensing systems: the TSG and the BGC-Argo floats. Systematic comparisons between the profiles from the CTD unit and the neighboring data were made at every cast.

Considering TSG data set, the median value of temperature and practical salinity over a time window of 1 h around the profile date was extracted from the 5 min resolution time series. The comparison with the surface value from profiles showed a spread distribution of misfits for temperature, with an average 0.009 °C, and a narrower distribution of misfits for practical salinity with an average of 0.007. Given the nominal accuracy expected by the TSG system and in absence of systematic marked shift in the comparison, no post-cruise adjustment was performed. The uncertainty of measurement in the TSG data set should have stayed under the 0.01 °C in temperature and 0.01 in practical salinity.

Considering BGC-Argo floats, the comparison with CTD profiles was performed over the 750–1000 dbar layer, where water mass characteristics remained stable enough to ascribe misfits as instrumental calibration shifts rather than natural variability. The misfits between temperature measurements and practical salinity measurements at geopotential horizons were computed and median values provided for every BGC-Argo float. The median offsets are reported in Table 2. Their amplitudes remained within 0.01 °C in temperature or 0.01 in practical salinity except in two cases. A large temperature offset occurred for WMO 6901769. A large practical salinity offset was reported for WMO 6901765, despite being deployed exactly concomitant with the CTD profile.

2.3 Oxygen concentration

2.3.1 Presentation of the different measurements

Concentration of dissolved dioxygen (O_2) in seawater, hereafter referred to as oxygen, was measured with three techniques: the classical iodometric Winkler method, an electrochemical oxygen sensor and optical oxygen sensors.

Oxygen concentration was measured following the Winkler method (Winkler, 1888) with potentiometric endpoint detection (Oudot et al., 1988) on discrete samples collected with Niskin bottles. For sampling, reagent preparation and analysis, the recommendations of Langdon (2010) were carefully followed.

Oxygen concentrations were measured by a Sea-Bird SBE43 (serial no. 0587) electrochemical sensor interfaced with the CTD unit. This sensor was plumbed in the pumped circuit following the GO-SHIP guidelines (Hood et al., 2010).

Oxygen optical measurements (also called optode measurements) were collected by two types of sensors. One Rinko III dissolved oxygen sensor from JFE Advanctech Co., Ltd., Japan (serial no. 171), was interfaced with the CTD

unit using the analog output voltage. Aanderaa 4330 optodes were mounted on every BGC-Argo float.

2.3.2 Data processing

The titration volumes were converted to oxygen concentrations in $\mu mol\,kg^{-1}$ by following the calculation procedure proposed in Langdon (2010). The precision of the Winkler measurements was estimated by reproducibility tests based on five or six replicates for samples withdrawn from the same Niskin bottles. The standard deviation of the replicate measurements was less than $0.4\,\mu mol\,kg^{-1}$.

The sensor signal of the SBE43 was aligned to temperature and pressure scans with an advanced offset considering a unique plumbing configuration for the cruise of 3 s. The raw signal was then converted to an oxygen concentration with 13 calibration coefficients. The method is based on the Owens and Millard (1985) algorithm that has been slightly adapted by Sea-Bird in the data processing software using a hysteresis correction (Sea-Bird Scientific, 2014). A new set of calibration coefficients for this sensor was determined after the cruise; it was used to post-process the whole data set. Only 3 (the oxygen signal slope, the voltage at zero oxygen signal and the pressure correction factor) of the 13 coefficients determined by the pre-cruise factory calibration of the sensor were adjusted with the following procedure. The oxygen concentrations measured by Winkler were matched with the signal measured by the sensor at the closing of the Niskin bottles. The three values were fitted by minimizing the sum of the square of the difference between Winkler oxygen and oxygen derived from sensor signal. Outliers were discarded when the residuals exceeded 2.8 standard deviation of the residuals until no more outliers remain.

The Rinko optode provided continuous voltage output at 24 Hz, which has been directly converted to an oxygen concentration with the MATLAB code developed by the manufacturer. The original calibration coefficients were used. To process the results, the temperature measured from the CTD unit was preferred to the built-in temperature of the sensor.

The Aanderaa optodes 4330 output signal is a C1 raw phase (phase from the blue light excitation), a C2 raw phase (phase from the red light excitation) and the optode temperature. The calculation of oxygen concentrations from the optode signal follows the recommendations of Thierry et al. (2016). The calibrated phase estimated from the C1 and C2 raw phases is converted in oxygen concentration by the Stern–Volmer equation proposed by Uchida et al. (2008) using seven calibration coefficients (the so-called Stern–Volmer–Uchida coefficients). The oxygen concentration is then corrected for salinity and pressure effects. The pressure compensation is estimated following Bittig et al. (2015) with a step of phase adjustment. Finally, concentrations are expressed in $\mu mol\,kg^{-1}$ by using the potential density derived from the CTD measurements of BGC-Argo floats.

2.3.3 Data quality control

Winkler measurements of discrete samples collected during upcasts were considered as the reference oxygen value because they rely on a reference material (KIO_3 standard) given with a precision of replicate measurements lower than $0.4\,\mu mol\,kg^{-1}$. The reference Winkler measurements were used to adjust the calibration coefficients of the CTD oxygen sensor (SBE43), as described below. The corrected oxygen profiles during downcasts from the SBE43 at stations were considered as the reference profile for optode measurements from BGC-Argo floats. This quality control was based on the downcast profiles at 1 dbar resolution collected either by the electrochemical sensor SBE43 or the optode RINKO.

Residuals with Winkler measurements were expressed as the difference in an isobaric horizon between the sensor oxygen and the Winkler oxygen. A sensor error was estimated as the root mean square error of the residuals. Results are reported in Fig. 2, where the residuals over the entire cruise are plotted as a function of time and depth. Residuals appear higher and more variable in the upper part of the water column, most probably due to enhanced oxygen gradients and changes on isobaric horizons between downcasts and upcasts. For electrochemical measurements, no significant offsets or drifts were observed; the sensor error over the entire cruise is $2.4\,\mu mol\,kg^{-1}$. For RINKO optode measurements, the sensor error over the entire cruise was $6.0\,\mu mol\,kg^{-1}$ and a systematic offset of $4.8\,\mu mol\,kg^{-1}$ was observed. Moreover, a significant increase of the residuals with depth ($0.0022\,\mu mol\,kg^{-1}\,dbar^{-1}$) was observed below 200 dbar. Thus, the SBE43 data were used rather than the RINKO data in the final record.

Considering BGC-Argo floats, it has been reported that a systematic shift in the optode calibration coefficients can occur during storage and shipment of the sensors (Bittig et al., 2012). In order to compensate for this potential shift, float oxygen measurements were corrected based on a reference profile as in Takeshita et al. (2013). A slope and offset value were determined for every optode deployed in order to adjust a posteriori the calculated oxygen values from the raw signals. The adjustment of optode values was performed using a linear model, below the first 50 dbar to avoid strong variability in the surface layer, and above the last 50 dbar to get rid of possible hooks at the bottom of profiles. The results, reported in Table 2, show a consistent correlation between the two sensors and offsets ranging from -14 to $11\,\mu mol\,kg^{-1}$.

2.4 Chlorophyll *a* concentration

2.4.1 Presentation of the different measurements

The chlorophyll *a* concentration (Chl *a*; sum of chlorophyll *a*, divinyl chlorophyll *a* and chlorophyllide *a*) in seawater was measured with two methods: high-performance liquid chromatography (HPLC) and fluorescence.

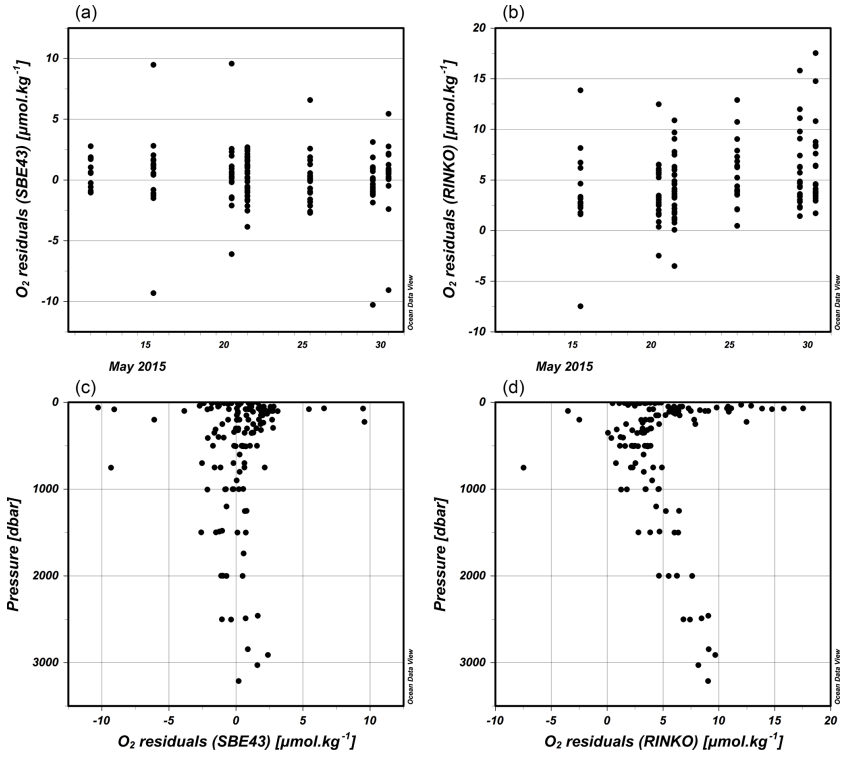

Figure 2. Oxygen residuals between sensor and Winkler measurements, plotted as a function of time **(a, b)** and as a function of depth **(c, d)**. The residuals for the electrochemical sensor are plotted in **(a, c)**, and those for the optode in **(b, d)**.

The HPLC method is used to estimate the Chl *a* in discrete seawater samples collected from the TSG system or withdrawn from Niskin bottles. For this, 2.27 L of the seawater samples was filtered onto glass fiber filters (GF/F Whatman 25 mm), and all filters were then stored in liquid nitrogen at −80 °C until further laboratory analysis. The chlorophyll *a* and other accessory phytoplankton pigments were then extracted from the filters in 100 % methanol, disrupted by sonification and clarified by filtration (GF/F Whatman 0.7 µm) after 2 h. Extracts were injected (within 24 h of beginning of the extraction) on a reversed-phase C8 column, and 24 pigments were separated, identified and quantified according to the HPLC analytical protocol described by Ras et al. (2008).

Fluorometers provide continuous detection of chlorophyll *a*. Three kinds of sensors were used during the cruise: Chelsea Aqua Tracka III fluorometer (serial no. 088193) interfaced with CTD unit, ECO WetLabs fluorometers that equipped every BGC-Argo float and a Turner fluorometer (serial no. 6241) plumbed in the TSG system of the vessel. The sensing mean is based on the fluorescence concept: irradiated by blue light, chlorophyll *a* absorbs and re-emits in the red part of the spectrum, and the re-emitted signal (i.e., the fluorescence) is considered proportional to the Chl *a* (Lorenzen, 1966). However, to retrieve the exact Chl *a* through the raw fluorescence signal, a calibration of the signal is necessary.

Note that fluorescence is affected by non-photochemical quenching, the protection mechanism employed by phytoplankton against the effects of high light intensity. As a result, amplitude of signal is reduced for an identical Chl *a* when the measurement is performed under sunlight exposure in the sea surface layer.

2.4.2 Data processing

The Chl *a* is derived from raw fluorescence signal by a linear model using two calibration coefficients: an offset that corresponds to the value of the signal in the absence of Chl *a* and a scaling factor to align the signal on the exact in situ Chl *a*. These calibration coefficients are generally provided by the manufacturer, but an adjustment using in situ measurements of Chl *a* is recommended. The calibration method was based on the alignment of the fluorescence signal to exact in situ discrete measurements of Chl *a* provided by the HPLC method. For this, a least square linear regression was used with simultaneous measurements of Chl *a* from fluorescence at the time, location and depth of collected seawater samples analyzed by HPLC. The statistics associated with the linear regression were used as a quality control of the calibration.

Fluorometer-derived Chl *a* profiles at CTD casts were processed as follows. As a pre-processing step, the raw fluorescence measurements were corrected for possible non-photochemical quenching following the procedure of Xing

Table 4. List of parameters in the pigment data set, variable names and units; for each pigment, the detection wavelengths and the associated limits of detection in nanograms per injection (ng/inj).

Pigment	Variable name	Units	Detection wavelength (nm)	Limit of detection (ng/inj)	Limit of detection for 2 L filtered (in mg m^{-3})
Chlorophyll c3	CHLC3	mg m^{-3}	450	0.015	0.0002
Chlorophyll c1 + c2	CHLC2	mg m^{-3}	450	0.018	0.0002
Sum chlorophyllide *a*	CHLDA	mg m^{-3}	667	0.016	0.0002
Peridinin	PERI	mg m^{-3}	450	0.007	0.0001
Sum phaeophorbid *a*	PHDA	mg m^{-3}	667	0.009	0.0001
19'-Butanoyloxyfucoxanthin	BUT	mg m^{-3}	450	0.009	0.0001
Fucoxanthin	FUCO	mg m^{-3}	450	0.009	0.0001
Neoxanthin	NEO	mg m^{-3}	450	0.009	0.0001
Prasinoxanthin	PRAS	mg m^{-3}	450	0.009	0.0001
Violaxanthin	VIOLA	mg m^{-3}	450	0.012	0.0001
19'-Hexanoyloxyfucoxanthin	HEX	mg m^{-3}	450	0.009	0.0001
Diadinoxanthin	DIADINO	mg m^{-3}	450	0.014	0.0002
Alloxanthin	ALLO	mg m^{-3}	450	0.015	0.0002
Diatoxanthin	DIATO	mg m^{-3}	450	0.015	0.0002
Zeaxanthin	ZEA	mg m^{-3}	450	0.014	0.0002
Lutein	LUT	mg m^{-3}	450	0.014	0.0002
Bacteriochlorophyll *a*	BCHLA	mg m^{-3}	770	0.010	0.0001
Divinyl chlorophyll *b*	DVCHLB	mg m^{-3}	450	0.004	0.0001
Chlorophyll *b*	CHLB	mg m^{-3}	450	0.004	0.0001
Total chlorophyll *b*	TCHLB	mg m^{-3}	450	0.004	0.0001
Divinyl chlorophyll *a*	DVCHLA	mg m^{-3}	667	0.011	0.0001
Chlorophyll *a*	CHLA	mg m^{-3}	667	0.011	0.0001
Total chlorophyll *a*	TCHLA	mg m^{-3}	667	0.011	0.0001
Sum phaeophytin *a*	PHYTNA	mg m^{-3}	667	0.007	0.0001
Sum carotenes	TCAR	mg m^{-3}	450	0.013	0.0002

et al. (2012). The linear regression was done with 61 simultaneous measurements of Chl *a* determined by HPLC and the fluorometer. The resulting coefficients were an offset of 0.168 mg m^{-3} and a slope of 4.016 with a coefficient of determination equal to 0.96. An alternative estimation of the offset was performed by computing the median value of raw fluorescence profiles in the last 50 m of every profile. Indeed, when the water column is stratified (it was always the case here), the availability of light is not enough to allow the presence of active phytoplankton cells; thus the fluorescence signal should be null. This estimation considering all the fluorescence profiles provides an offset of 0.160 ± 0.004 mg m^{-3}.

As for CTD casts, the raw fluorescence measurements from BGC-Argo floats were corrected for possible non-photochemical quenching, and offsets were determined as median values of raw fluorescence in the last 50 m of the profiles. The estimated offset values are reported in Table 2. Once offsets were adjusted, the linear regressions were performed with seven or eight simultaneous measurements of Chl *a* obtained by HPLC at the float deployment. The estimated slopes are reported in Table 2. On average from all the calibration conducted, slopes range from 0.49 to 0.67 with an average value of 0.58; offsets range from −0.02 to 0.04 mg m^{-3} with an average value of 0.02 mg m^{-3}.

Considering fluorometer-derived Chl *a* along the ship track, a post-cruise estimation of the calibration coefficients for the Turner fluorometer was undertaken. The linear regression was done with nine discrete seawater samples collected at night (between 19:00 and 05:00 UTC) to avoid the non-photochemical quenching. The calibration coefficients obtained were an offset of 0.059 mg m^{-3} and a slope of 4.831 with a coefficient of determination equal to 0.70. The raw fluorescence measurements were included in the TSG data flow of 15 s resolution. The TSG data processing followed the same steps as for ship-track temperature and salinity, to provide average time series in 5 min bins.

2.4.3 Data quality control

In the Table 4, the list of quantified pigments and their limits of detections (calculated in nanograms per injection and as the concentrations corresponding to a signal-to-noise ratio of 3) is provided. Different quality control steps were applied

during HPLC analysis, data processing and to the final data set. During HPLC analysis, parameters such as the stability of the baseline, the injection precision and the pressure were monitored regularly in order to detect potential anomalies in the analytical process. During data processing, chromatographic parameters were checked, including critical pair resolution, baseline noise and peak width or retention time precision. Spectral data for the different peaks were verified and used for identification purposes and peak purity assessment. The final pigment database underwent a visual verification step for each pigment of every vertical profile and quality flags were assigned for each value. The visual check confirms that the identification and quantification of all the samples did not present any issues, such as coelution problems or baseline noise leading to potential uncertainties.

Considering fluorescence measurements collected on CTD casts, the high coefficient of determination ($r^2 = 0.96$) for the linear model denotes a very good regression with HPLC data. The pair of calibration coefficients were applied in the post-processing of fluorescence data at every cast.

Considering fluorescence measurements collected by BGC-Argo floats, good alignment with in situ data was reached with coefficients of determination higher than 0.75 (see Table 2). Moreover, the homogeneity of slopes among the series of new sensors (thus recently factory calibrated) gives insight into the gain (between 1.8 and 2) to be applied afterwards to fluorescence data (Roesler et al., 2017).

Considering fluorescence measurements collected on the TSG system, its range along the ship track appears very narrow (from 0.035 to 0.112 mg m^{-3}). In addition, a low number of simultaneous HPLC measurements is available (only nine samples), and the coefficient of determination of the linear regression is lower than 0.70. Thus, the calibration effort performed is certainly not enough to provide full confidence in the adjusted coefficients, although they have been applied to the TSG time series.

2.5 Nitrate (and other nutrient) concentrations

2.5.1 Presentation of the different measurements

Concentrations of nitrate (NO_{3-}) ions in seawater were measured with two techniques: the classical colorimetric method in conjunction with nitrite, phosphate and silicate concentrations, and with an optical nitrate sensor.

Nutrient samples were collected and conserved following the recommendations of Kirkwood (1992). All nutrient samples were analyzed by a standard automated colorimetric system set up following Aminot and Kerouel (2007), using a Seal Analytical continuous flow AutoAnalyzer III (AA3).

Optical sensor measurements were performed on BGC-Argo floats. Sensors using miniaturized ultraviolet spectrophotometers allow for continuous measurement of absorbance spectra and estimations of nitrate concentrations (Johnson and Coletti, 2002). The BGC-Argo floats deployed during this cruise were equipped with the Satlantic SUNA-V2 (Submersible Ultraviolet Nitrate Analyzer) sensors.

2.5.2 Data processing

Nitrate concentrations are derived from absorbance spectra using the TCSS (temperature compensated, salinity subtracted) algorithm developed by Sakamoto et al. (2009). In the Mediterranean Sea, because of specific conditions of low nitrate concentrations and high salinity (thus high bromide concentrations), optical measurements of nitrate were extremely delicate (D'Ortenzio et al., 2014). This drove the development of a specific algorithm adapted from TCSS that substantially improved the estimation of nitrate concentrations in this area (Pasqueron de Fommervault et al., 2015).

The BGC-Argo floats deployed during the cruise transmitted the raw data of the SUNA (i.e., absorbance spectrum from 217 to 250 nm), which allowed for post-processing with the algorithm of Pasqueron de Fommervault et al. (2015). A spike test was applied in addition to a test for saturation based on the raw absorption spectrum. Nitrate concentration data computed from a spectrum for which more than 25 % of the channels saturate (i.e., reached the maximum value of numerical counts) were discarded. This was the case of one BGC-Argo float (WMO6901773).

2.5.3 Data quality control

The SUNA sensors also undergo offset and gain (Johnson et al., 2013) that were corrected using as reference the measurements of discrete samples. Given that surface nitrate concentrations in May and June in the Mediterranean Sea are below the limit of detection of the sensor (Pasqueron de Fommervault et al., 2015), an offset was computed as the difference between an assumed surface concentration of zero and the mean nitrate value measured from 5 to 30 m. A gain was then calculated with a match up between sensors measurements and nitrate concentrations at discrete depths. Gain correction was applied only if the misfits between sensor derived and reference concentrations below 950 dbar did not exceed 10 % of the deep reference value. The correction coefficients per BGC-Argo float are reported in Table 2. A slope of 1 was estimated for most of the cases, and the offsets ranged from -2.70 to 3.90 µ mol L^{-1}.

3 Data availability

The final data set concatenates the different collections during the cruise, which are vertical profiles and bottle samples at CTD casts and along-track measurements at surface and at depth. This data set benefits from post-cruise corrections described in the previous sections. A unique convention was used to identify bad, absent or unreported data: they have been assigned the value -999.

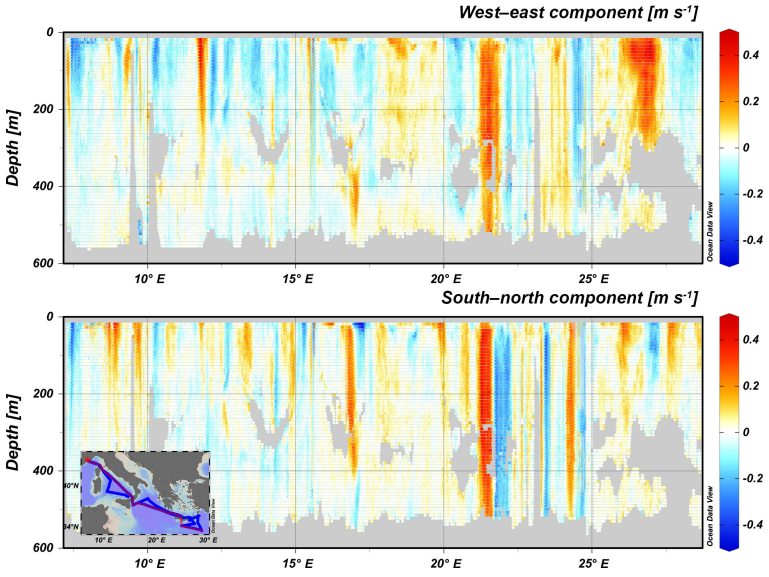

Figure 3. Velocity distribution of the upper water column along a west–east section through the Mediterranean Sea. Data are recorded by SADCP. Inner panel indicates the location of the ship track and the section. Grey areas: no data are available.

The quality control applied to discrete sample collection has been assigned with a quality flag. The quality code developed for WHP bottle parameters data was used, in particular "2: Acceptable measurement", "5: Not reported" and "9: Sample not drawn for this measurement from this bottle".

Data are published by SEANOE operated by SISMER within the framework of the information system ODATIS. Data from the stations are available at https://doi.org/10.17882/51678 (Taillandier et al., 2017a), data along the ship track are available at https://doi.org/10.17882/51691 (Taillandier et al., 2017b).

4 Discussion and conclusions

With an extension of about 25° in longitude, this cruise covered the central Mediterranean Sea and part of its northwestern and eastern basins. High-resolution ADCP data (Fig. 3) reveals some well-known patterns of the surface circulation in this area (the cyclonic gyre in the Ligurian Basin, the eastward surface flow in the Levantine) as well as ubiquitous mesoscale activity. Seven stations were chosen in this transect (one in the Ligurian, two in the Tyrrhenian, two in the Ionian, two in the Levantine) in order to provide a large-scale record on the hydrography and biogeochemistry of the Mediterranean Sea. As shown in Fig. 4a, there is a clear separation of water mass characteristics between the eastern and western basin, with a clear longitudinal gradient as deep waters and intermediate waters become saltier and warmer eastwards. Associated with this water mass distribution, biogeochemical traits clearly showed important differences among basins and relative homogeneity within basins. As shown in Fig. 4c, the oxygen minimum of the intermediate waters is the lowest in the western stations, and deep waters are more oxygenated in basins directly influenced by winter convection (Ligurian and Ionian). The nutrient distribution also shows the eastern depletion of nitrates in deep waters, shallower nitraclines in the western basin and the absence of nitrates in the surface layers relevant to the Mediterranean oligotrophic spring regime (see Fig. 4d). These large-scale patterns are in good agreement with observations reported by previous field surveys such as BOUM in 2009 (Moutin and Prieur, 2012) or M84/3 in 2011 (Tanhua et al., 2013). Consequently, the vertical distribution of biomass is marked by a deep chlorophyll maximum; this maximum becomes higher and shallower between the eastern to western basins (see Fig. 4b). Such spatial contrasts need to be complemented by the temporal evolution of these patterns which can be achieved thanks to the BGC-Argo floats.

The data set presented in this paper has been collected in the framework of an emerging in situ observing system in the Mediterranean Sea. In order to characterize the seasonal cycles of phytoplankton dynamics and the biogeochemical functioning of the Mediterranean Sea, this network of twelve BGC-Argo floats collects data on physical and biogeochemical properties (temperature, salinity, concentration of dissolved oxygen, chlorophyll *a*, nitrate) along 1000 m depth profiles at a weekly sampling rate. In spring 2015, shipboard measurements were acquired with the objective of providing a reference data set for each core parameter of the in situ observing system, verified through the inter-comparison of several in situ sensing methods. This data set allowed performing metrological verification of the deployed sensors, considering the misfits between the first profile of the float and the shipboard data. This data set can provide ancillary data

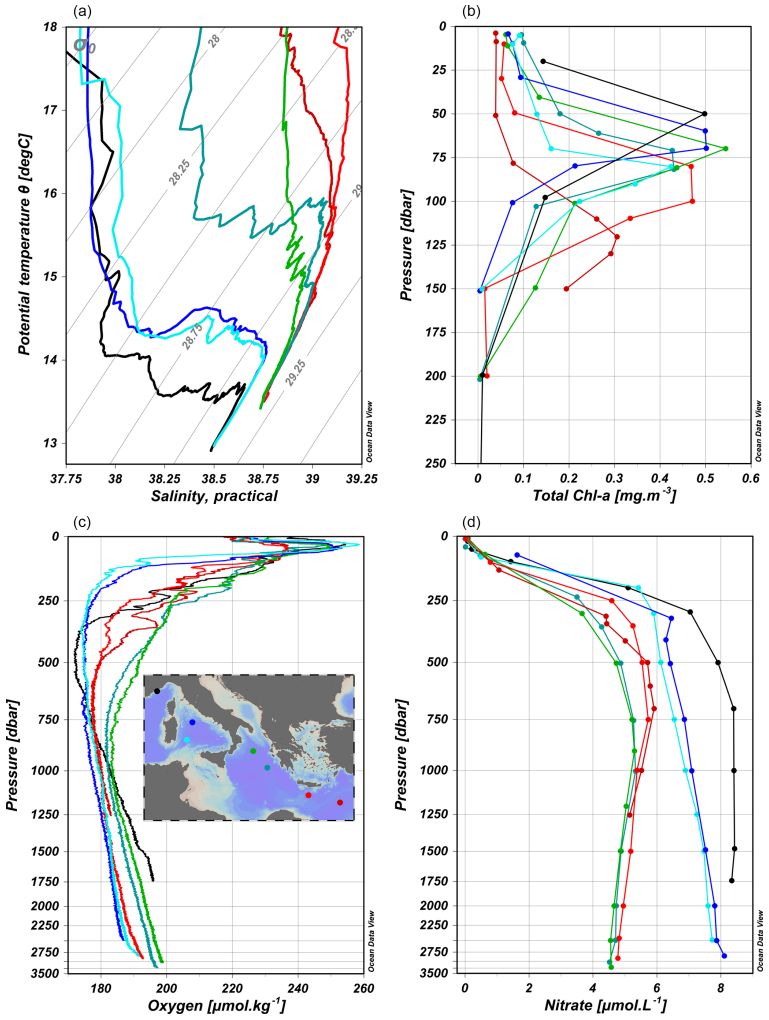

Figure 4. TS diagram comprised of CTD data **(a)**; total chlorophyll *a* concentration profiles by HPLC method **(b)**; dissolved oxygen concentration profiles from CTD data **(c)**; nitrate concentration profiles by colorimetric method **(d)**. The inner panel shows the locations of CTD stations.

for performing and distributing delayed-mode adjustments in the time series of these BGC-Argo floats to end users (e.g., Schmechtig et al., 2015).

First, the presented data set provides an in situ characterization of the environmental conditions in which the verification exercises were conducted. Thanks to ocean current and surface hydrography information collected along the ship track, a first assessment of the circulation patterns neighboring every station can be made. Complemented with satellite observations (altimetry, images of sea surface temperature or ocean color), the degree of stability of the water column can be diagnosed in order to relate (or not) the co-location in space and time of the BGC-Argo float profile with reference data.

Second, the presented data set provides material for the systematic calibration of the biogeochemical sensors active in the network. The crucial role of this operation on newly deployed sensors has been shown (Table 2). Concerning the oxygen optode sensors, their linear response does not seem to be affected; however, offsets reaching amplitudes of 15 µmol kg^{-1} have been reported, without any systematic bias among the set of sensors. Concerning fluorometer sensors, offsets can be corrected considering dark values at depth; however, the amplitudes of the signals appeared to be overestimated by a factor between 1.5 and 2 depending on the sensor. Concerning nitrate sensors, their behavior at deployment is similar to the optodes in terms of calibration, with a sensor-dependent offset up to 4 µmol L^{-1} of amplitude. Overall, the biogeochemical sensors equipped on the BCG-Argo floats revealed inherent calibration shifts upon deployment. This is in agreement with recent works on ECO fluorometers (Roesler et al., 2017) and oxygen optodes (Bittig et al., 2015; Bittig and Körtzinger, 2015).

The data set presented is relevant for the robust evaluation of the calibration state of biogeochemical sensors at the beginning of their mission. In addition, if an equivalent data set is collected at the end of the mission when the BGC-Argo floats are recovered, the sensor drifts can be properly assessed from pre-mission and post-mission calibration states. This objective appears essential to allow for the harmonization between all the time series observed by the network.

This data set is a first attempt at evaluating the uncertainties that come up in the verification exercises. When measuring misfits between shipboard measurements and the first profile of the BGC-Argo floats, the natural variability of the environment can affect their complete attribution to calibration shifts. This natural variability can be inferred by diurnal cycles for biogeochemical sensors, or to a lesser extent by mesoscale effects. The expected variations depend on the type of parameter, the depth of inter-comparison and the duration or distance between profiles. Among the BGC-Argo floats deployed during the cruise, two benefited from a perfectly concomitant verification exercise, as they were clamped onto the CTD carousel. The first results show reduced dispersion as a function of depth for all the parameters. This dispersion criterion needs to be assessed more carefully with different types of match up, as a function of local environmental conditions and duration or distance from the first profile.

Preliminary conclusions stress the importance of evaluating the calibration state of the biogeochemical sensors and their possible drift over several mission years. The data set collected during the cruise of May 2015 provided relevant material for performing such metrological verification exercises, and justifies future deployments. The cruise also unintentionally showed it was possible to perform predeployment verification exercises some days before the beginning of the mission. The floats with newly verified sensors were deployed close to those recovered in order to continue their time series and to retrieve post-mission calibration states. If the propagation of reference data between missions is satisfactory, such a protocol could be applied to conventional oceanographic cruises as they demand one station of metrological verification with floats mounted on the CTD carousel and changes of route for float deployment and recovery operations.

Author contributions. This data set was collected by VT, TW, FDO, HLG and NM. TW analyzed the oxygen samples, JR analyzed the pigment samples, and ED analyzed the nutrient samples. Data processing and quality control were undertaken by HLG for ocean currents and TSG; by VT for seawater hydrological properties; by FDO and NM for chlorophyll *a* concentration; by TW, LC, HB and DL for oxygen concentration; and by OPF and FDO for nitrate concentration. VT, AP and EL organized the BGC-Argo float deployments and recoveries. Data management and availability were undertaken by CS. VT and TW prepared the manuscript with contributions from FDO, NM, JR, LP and OPF.

Competing interests. The authors declare that they have no conflict of interest.

Acknowledgements. We would like to thank Captain Dany Deneuve and the crew of RV *Tethys 2*. These observational efforts were supported the project Equipex-NAOS, the Euro-Argo infrastructure, the program MerMex, and the project BAMA funded by LEFE/GMMC. We gratefully acknowledge their support.

Edited by: Giuseppe M. R. Manzella
Reviewed by: two anonymous referees

References

Aminot, A. and Kerouel, R.: Dosage automatique des nutriments dans les eaux marines methodes en flux continu, in: Methodes d'analyse en milieu marin, Ifremer, Editions 25 Quae, 188 pp., 2007.

Bittig, H. C. and Körtzinger A.: Tackling Oxygen Optode Drift: Near-Surface and In-Air Oxygen Optode Measurements on a Float Provide an Accurate in Situ Reference, J. Atmos. Ocean. Tech., 32, 1536–1543, https://doi.org/10.1175/JTECH-D-14-00162.1, 2015.

Bittig, H. C., Fiedler, B., Steinhoff, T., and Körtzinger A.: A novel electrochemical calibration setup for oxygen sensors and its use for the stability assessment of Aanderaa optodes, Limnol. Oceanogr.-Meth., 10, 921–933, https://doi.org/10.4319/lom.2012.10.921, 2012.

Bittig, H. C., Fiedler, B., Fietzek, P., and Körtzinger, A.: Pressure response of Aanderaa and Sea-Bird oxygen optodes, J. Atmos. Ocean. Tech., 32, 2305–2317, https://doi.org/10.1175/JTECH-D-15-0108.1, 2015.

Bosc, E., Bricaud, A., and Antoine, D.: Seasonal and interannual variability in algal biomass and primary production in the Mediterranean Sea, as derived from four years of SeaWiFS observations, Global Biogeochem. Cy., 18, GB1005, https://doi.org/10.1029/2003GB002034, 2004.

D'Ortenzio, F. and Ribera d'Alcalà, M.: On the trophic regimes of the Mediterranean Sea: a satellite analysis, Biogeosciences, 6, 139–148, https://doi.org/10.5194/bg-6-139-2009, 2009.

D'Ortenzio, F., Lavigne, H., Besson, F., Claustre, H., Coppola, L., Garcia, N., and Morin, P.: Observing mixed layer depth, nitrate and chlorophyll concentrations in the northwestern Mediterranean: A combined satellite and NO3 profiling floats experiment, Geophys. Res. Lett., 41, 6443–6451, 2014.

Durrieu de Madron, X., and the MerMex group: Marine ecosystems' responses to climatic and anthropogenic forcings in the Mediterranean, Prog. Oceanogr., 91, 97–116, 2011.

Giorgi, F. and Lionello, P.: Climate change projections for the Mediterranean region, Global Planet. Change, 63, 90–104, 2008.

Hood, E. M., Sabine, C. L., and Sloyan B. M.: The GO-SHIP repeat hydrography manual: A collection of expert reports and guide-

lines, IOCCP Report No.14, ICPO Publication Series No. 134, Version 1, 2010.

Johnson, K. S. and Coletti, L. J.: In situ ultraviolet spectrophotometry for high resolution and long-term monitoring of nitrate, bromide and bisulfide in the ocean, Deep-Sea Res. Pt. I, 49, 1291–1305, 2002.

Johnson, K. S., Coletti, L. J., Jannasch, H. W., Sakamoto, C. M., Swift, D. D., and Riser, S. C.: Long-term nitrate measurements in the ocean using the In Situ Ultraviolet Spectrophotometer: sensor integration into the Apex profiling float, J. Atmos. Ocean. Tech., 30, 1854–1866, 2013.

Johnson, K. S., Plant, J. N., Coletti L. J., Jannasch, H. W., Sakamoto C. M., Riser, S. C., Swift, D. D., Williams, N. L., Boss, E., Lynne, N. H., Talley, D., and Sarmiento, J. L.: Biogeochemical sensor performance in the SOCCOM profiling float array, J. Geophys. Res.-Oceans, 122, 6416–6436, https://doi.org/10.1002/2017JC012838, 2017.

Kirkwood, D. S.: Stability of solutions of nutrient salts during storage, Mar. Chem., 38, 151–164, 1992.

Langdon, C.: Determination of Dissolved Oxygen in Seawater by Winkler Titration Using the Amperometric Technique In The GO-SHIP Repeat Hydrography Manual, in: A Collection of Expert Reports and Guidelines, edited by: Hood, E. M., Sabine, C. L., and Sloyan, B. M., IOCCP Report Number 14, ICPO Publication Series Number 134, available at: http://www.go-ship.org/HydroMan.html (last access: 22 March 2018), 2010.

Le Bot, P., Kermabon, C., Lherminier, P., and Gaillard, F.: Cascade V6.1: Logiciel de validation et de visualization des mesures ADCP de coque, document utilisateur et maintenance, Report OPS/LPO 11-01, 2011.

Leymarie, E., Poteau, A., André, X., Besson, F., Brault, P., Claustre, H., David, A., D'Ortenzio, F., Dufour, A., Lavigne, H., Reste, S. L., Le Traon, P. Y., Migon, C., Nogre, D., Obolensky, G., Penkerc'h, C., Sagot, J., Schaeffer, C., Schmechtig, C., and Taillandier, V.: Development and validation of the new ProvBioII float, Mercator Ocean Quarterly Newsletter, available at: https://www.mercator-ocean.fr/wp-content/uploads/2015/05/Mercator-Ocean-newsletter-2013_48.pdf, 2013.

Lorenzen, C. J.: A method for the continuous measurement of in vivo chlorophyll concentration, Deep Sea Res. Oceanogr. Abstr., 13, 223–227, https://doi.org/10.1016/0011-7471(66)91102-8, 1966.

Marty, J. C. and Chiavérini, J.: Hydrological changes in the Ligurian Sea (NW Mediterranean, DYFAMED site) during 1995–2007 and biogeochemical consequences, Biogeosciences, 7, 2117–2128, https://doi.org/10.5194/bg-7-2117-2010, 2010.

Marty, J. C., Chiaverini, J., Pizay, M. D., and Avril, B.: Seasonal and interannual dynamics of nutrients and phytoplankton pigments in the western Mediterranean Sea at the DYFAMED time-series station (1991–1999), Deep-Sea Res. Pt. II, 49, 1965–1985, 2002.

Mayot, N., D'Ortenzio, F., Ribera d'Alcalà, M., Lavigne, H., and Claustre, H.: Interannual variability of the Mediterranean trophic regimes from ocean color satellites, Biogeosciences, 13, 1901–1917, https://doi.org/10.5194/bg-13-1901-2016, 2016.

Moutin, T. and Prieur, L.: Influence of anticyclonic eddies on the Biogeochemistry from the Oligotrophic to the Ultraoligotrophic Mediterranean (BOUM cruise), Biogeosciences, 9, 3827–3855, https://doi.org/10.5194/bg-9-3827-2012, 2012.

Oudot, C., Gerard, R., Morin, P., and Gningue, I.: Precise shipboard determination of dissolved-oxygen (Winkler Procedure) with a commercial system, Limnol. Oceanogr., 33, 146–150, 1988.

Owens, W. B. and Millard Jr., R. C.: A new algorithm for CTD oxygen calibration, J. Phys. Oceanogr., 15, 621–631, 1985.

Pasqueron de Fommervault, O., D'Ortenzio, F., Mangin, A., Serra, R., Migon, C., Claustre, H., Lavigne, H. Ribera d'Alcalà, M., Prieur, L., Taillandier, V., Schmechtig, C., Poteau, A., Leymarie, E., Besson, F., and Obolensky, G.: Seasonal variability of nutrient concentrations in the Mediterranean Sea: Contribution of Bio-Argo floats, J. Geophys. Res.-Oceans, 120, https://doi.org/10.1002/2015JC011103, 2015.

Ras, J., Claustre, H., and Uitz, J.: Spatial variability of phytoplankton pigment distributions in the Subtropical South Pacific Ocean: comparison between in situ and predicted data, Biogeosciences, 5, 353–369, https://doi.org/10.5194/bg-5-353-2008, 2008.

Roesler, C., Uitz, J., Claustre, H., Boss, E., Xing, X., Organelli, E., Briggs, N., Bricaud, A., Schmechtig, C., Poteau, A., D'Ortenzio, F., Ras, J., Drapeau, S., Haëntjens, N., and Barbieux, M.: Recommendations for obtaining unbiased chlorophyll estimates from in-situ chlorophyll fluorometers: A global analysis of WET Labs ECO sensors, Limnol. Oceanogr.-Meth., 15, 572–585, https://doi.org/10.1002/lom3.10185, 2017.

Sakamoto, C. M., Johnson, K. S., and Coletti, L. J.: Improved algorithm for the computation of nitrate concentrations in seawater using an in situ ultraviolet spectrophotometer, Limnol. Oceanogr.-Meth., 7, 132–143, 2009.

Schmechtig, C., Poteau, A., Claustre, H., D'Ortenzio, F., and Boss, E.: Processing bio-Argo chlorophyll-a concentration at the DAC level, Argo data management, https://doi.org/10.13155/39468, 2015.

Sea-Bird Scientific: Application Note 64-3: SBE 43 dissolved oxygen (DO) sensor – hysteresis corrections, available at: http://www.seabird.com/document/an64-3-sbe-43-dissolved-oxygen-do-sensor-hysteresis-corrections (last access: 22 March 2018), 2014.

Siokou-Frangou, I., Christaki, U., Mazzocchi, M. G., Montresor, M., Ribera d'Alcalà, M., Vaqué, D., and Zingone, A.: Plankton in the open Mediterranean Sea: a review, Biogeosciences, 7, 1543–1586, https://doi.org/10.5194/bg-7-1543-2010, 2010.

Taillandier, V., Wagener, T., D'Ortenzio, F., Mayot, N., Legoff, H., Ras, J., Coppola, L., Pasqueron de Fommervault, O., Bittig, H., Lefevre, D., Leymarie, E., Schmechtig, C., and Poteau, A.: Oceanographic dataset in the Mediterranean Sea collected during the cruise BioArgoMed 2015, https://doi.org/10.17882/51678, 2017a.

Taillandier, V., Wagener, T., D'Ortenzio, F., Mayot, N., Legoff, H., Ras, J., Coppola, L., Pasqueron de Fommervault, O., Bittig, H., Lefevre, D., Leymarie, E., Schmechtig, C., and Poteau, A.: Ship-track continuous dataset in the Mediterranean Sea collected during the cruise BioArgoMed 2015, https://doi.org/10.17882/51691, 2017b.

Takeshita, Y., Martz, T. R., Johnson, K. S.,Plant, J. N., Gilbert, D., Riser, S. C., Neill, C., and Tilbrook, B.: A climatology-based quality control procedure for profiling float oxygen data, J. Geophys. Res.-Oceans, 118, 5640–5650, https://doi.org/10.1002/jgrc.20399, 2013.

Tanhua, T., Hainbucher, D., Schroeder, K., Cardin, V., Álvarez, M., and Civitarese, G.: The Mediterranean Sea system: a review and

an introduction to the special issue, Ocean Sci., 9, 789–803, https://doi.org/10.5194/os-9-789-2013, 2013.

Thierry V., Gilbert D., Kobayashi T., Schmid C., and Kanako S.: Processing Argo oxygen data at the DAC level cookbook, Argo data management, https://doi.org/10.13155/39795, 2016.

Thurnherr, A. M.: How to process LADCP data with the LDEO Software (Versions IX.7-IX.10), Internal report, March 2014.

Uchida, H., Kawano, T., Kaneko, I., and Fukasawa, M.: In situ calibration of optode-based oxygen sensors, J. Atmos. Ocean. Tech., 25, 2271–2281, https://doi.org/10.1175/2008JTECHO549.1, 2008.

Winkler, L. W.: Die Bestimmung des im Wasser gelosten Sauerstoffes, Ber. Dtsch. Chem. Ges, 21, 2843–2853, 1888.

Xing, X., Claustre, H., Blain, S., D'Ortenzio, F., Antoine, D., Ras, J., and Guinet, C.: Quenching correction for in vivo chlorophyll fluorescence acquired by autonomous platforms: A case study with instrumented elephant seals in the Kerguelen region (Southern Ocean), Limnol. Oceanogr.-Meth., 10, 483–495, 2012.